# 8
# Coulomb's failure equation and the choice of strength parameters

## 8.1 Coulomb's Failure Equation

The past three chapters have developed stress – strain theories for soil: they have also recognized that in the general progress of deformation there will be a 'peak' stress at which a stress-controlled system can fail because of the state of an element of soil within the system. The question of the state of soil at peak stress was discussed in the first source of soil mechanics — the paper[1] by Coulomb in 1776.

Coulomb considered, Fig. 8.1(a), that soil was a rigid homogeneous material which could rupture into separate blocks. These blocks remained in contact but slid relative to each other along the contact surface. Coulomb observed such rupture surfaces in soil and rock. His experiments on solid rock specimens and on mechanisms with sliding contact suggested that both cohesion and friction must be overcome during slip along the rupture surface, Fig. 8.1(b). We follow Sokolovski and denote cohesion by ***k*** and angle of friction by $\boldsymbol{\rho}$ in order to ease the introduction to his text. (In general, symbols $(c,\phi)$ are used, but these have over the years become very confused by innumerable definitions and suffices.) If we call the effective stress component across the rupture surface $\sigma'$, then the shearing stress $\tau$ that is available to resist motion along the rupture surface is written

$$|\tau| \le k + \sigma' \tan \boldsymbol{\rho}. \tag{8.1}$$

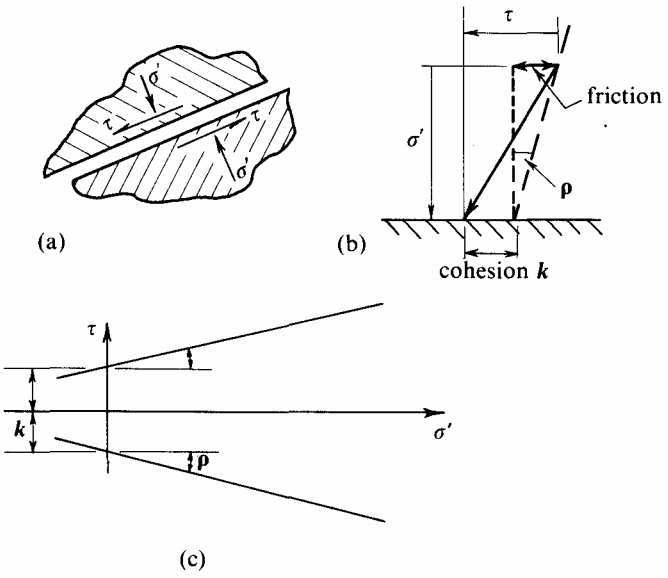


Fig. 8.1 Coulomb's Failure Criterion

This is the 'Coulomb equation': it is implicit in Coulomb's derivation of another eq. (9.5) to which we will come later, although it was not written explicitly in the 1776 paper.

For engineers 'classical' soil mechanics is the extensive set of design calculations and studies which is based on eq. (8.1). These studies reach their highest development in the recent text of Sokolovski on the limiting equilibrium of soil which are discussed with

other calculations of limiting equilibrium in chapter 9. Before we introduce these classical calculations we must decide what values of $k$ and $\rho$ to choose for each soil.

In this chapter we will meet two quite distinct sets of values of $(k,\rho)$. The first set will be discussed in sections 8.2 to 8.4 where we are concerned with the experimental fact that data of *peak* strengths of soil specimens do fit a modified form of the Coulomb equation. However, in §8.5 we explain that it would be incorrect to use these 'peak' values $(k,\rho)$ in design calculations, because strength falls from its peak to lower values after failure. The second set of values $(k,\rho)$ that can be used rationally in design calculations are discussed in sections 8.6 to 8.8, which follows the rationale given by Bishop and Bjerrum[2] in 1960. It does seem that this choice of a second set of values $(k,\rho)$ for design is consistent with our use of the critical state model and we will call these rationally chosen design values the *critical state* strengths.

## 8.2 Hvorslev's Experiments on the Strength of Clay at Failure

Studies of the strength of clay specimens in Terzaghi's laboratory in Vienna succeeded in fusing together the concept of effective stress and Coulomb's concept of failure. We have already explained how Rendulic correctly generalized the effective stress concept, and now we outline Hvorslev's work.

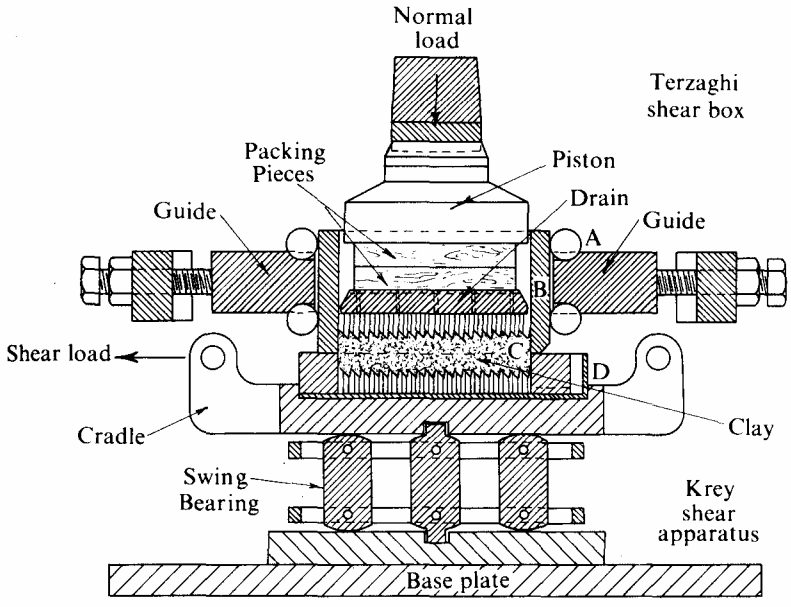


Fig. 8.2 Shear Apparatus used by Hvorslev

We know from the previous chapters 4, 5, and 6, that the specific volume of soil changes under changing effective stress, and we also know that yield strengths vary with specific volume. Equation (8.1), as it stands, takes no account of this change, and it was in elucidation of this point that the notable experiments of Hvorslev[3] made such a significant contribution.

Hvorslev used shear boxes of Terzaghi's design in a shear apparatus with a rocking cradle of Krey's design, as shown in Fig. 8.2. Clay specimens were consolidated from a slurry and brought into equilibrium under various normal loads. They were then subjected to successive increments of shear load: the experiments which we quote were very slow stress-controlled drained tests. Hvorslev defined 'failure' to be occurring under that shear

stress for which the very slow rates of shear displacement showed signs of continued acceleration.

Immediately after failure the shear boxes were quickly dismantled. A strip 3 mm thick and 2 cm wide was cut from the middle of the failure zone, as shown in Fig. 8.3; it was divided into five parts and the average water content for the zone of failure was determined. Observation of the rise or fall of the upper porous stone also indicated dilation or compression of the clay specimen during shear *before* failure.

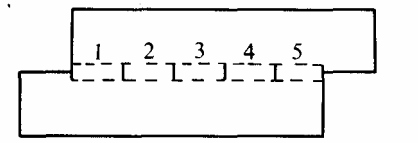


Fig. 8.3 Specimens for Determination of Final Water Content

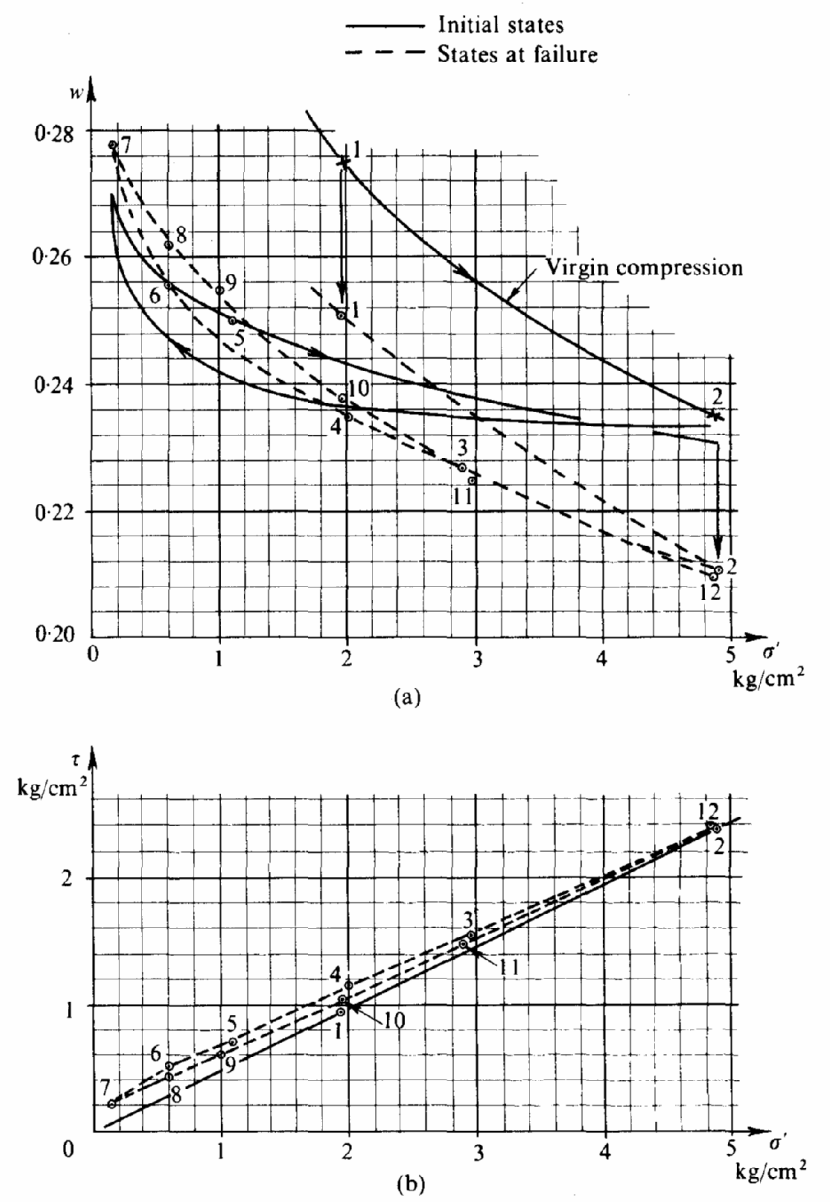


Fig. 8.4 Failure States of Specimens of Wiener Tegel V (After Hvorslev)

In Fig. 8.4(a) the solid line indicates a cycle of virgin compression, swelling, and recompression on a silty clay (Wiener Tegel V) said to resemble London clay. A dozen specimens were prepared each at a different stage in this cycle. Each specimen was then

sheared. Some exhibited a loss of water and others a gain during distortion. For all twelve specimens the circled dots indicate their state immediately after failure. A dashed line is drawn to link these points but this does not mean that a specimen changes; for instance, from the state at failure for 1 to the state at failure for 2. In Fig. 8.4(b) the set of failure strengths of these specimens is shown.

The data of Fig. 8.4 appear confusing, but Hvorslev introduced a major simplification. In Fig. 8.5 we re-plot the dashed curves of Fig. 8.4 together with the solid curve for virgin compression. For each water content on the dashed curve we read at the same water content on the solid curve a normal pressure which Hvorslev called the equivalent compressive pressure $\sigma'_e$; for clarity, only points 1, 4, and 7 are shown. Hvorslev found the equivalent pressures and replotted the data of Fig. 8.4(b) in the form of Fig. 8.6. All data lie on one straight line

$$\frac{\tau}{\sigma'_e} = k_0 + \frac{\sigma'}{\sigma'_e}\tan\rho_0 \qquad (8.2)$$

Introducing an equation for the virgin compression curve (in which $l$ is an appropriate constant)

$$\left.\begin{aligned} & w - w_0 = -l\ln\sigma'_e \\ \text{or} \quad & \sigma'_e = \frac{\exp(w_0 - w)}{l} \end{aligned}\right\} \qquad (8.3)$$

we obtain an alternative form

$$\left.\begin{aligned} & \tau = k + \sigma'\tan\rho_0 \\ \text{where} \quad & k = k(w) = \frac{k_0 \exp w_0}{l}\exp(-w) \end{aligned}\right\} \qquad (8.4)$$

These equations (8.4) elucidate a major significance of the Coulomb equation: it is that the cohesion component ***k*** increases exponentially with decrease of water content.

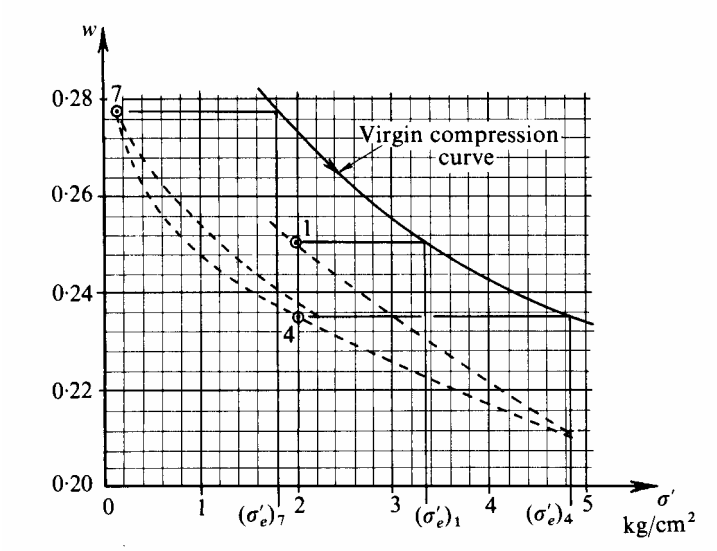


Fig. 8.5 Derivation of Equivalent Pressure (After Hvorslev)

This excellent set of accurate data was not subject to sufficiently close scrutiny by subsequent workers. It was not appreciated that the phenomenon that Hvorslev called failure was only observed in a limited range of states of soil: for Wiener Tegel V in Fig. 8.7 the range II is $0.05 < (\sigma'/\sigma'_e) < 0.6$ and it is most striking[4] that in range I for

$0.6 < (\sigma'/\sigma'_e)$ *no* failure was observed. There is an accumulation of points at the end C of the line on the boundary between regions I and II**;** in the light of the work of previous chapters we readily see that C indicates the near vicinity of the critical state. Specimens originally in region I, being wetter than critical, will have moved through that region in process of yielding without failure; not until they approach the critical states will failure have terminated the yielding process.

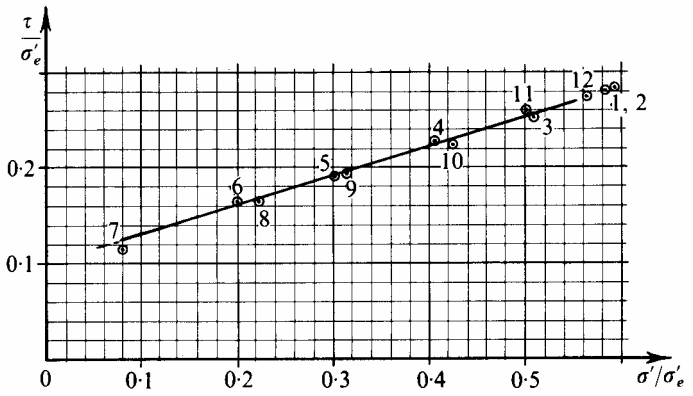


Fig. 8.6 Data of Failure (Wiener Tegel V) (After Hvorslev)

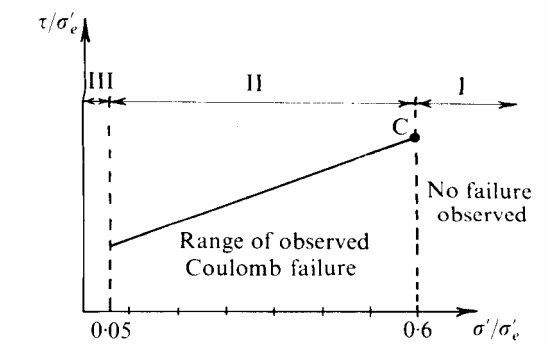


Fig. 8.7 Range of Observed Data of Failure

It is therefore clearly wrong to represent Hvorslev's results in the manner shown in Fig. 8.8(a), as some workers have done. It is wrong to consider the line OC to represent successive states of plastic compression in the presence of shear. In the near vicinity of the critical states plastic *distortion* increments are very large and no presently available test apparatus can hold a specimen in a condition close to the critical states sufficiently long for any controlled plastic *compression* to be imposed. It is also wrong to extend the lines of eq. (8.4) across the line OC into region I where Hvorslev did not obtain data of failure. A correct way to represent Hvorslev's equation is shown in Figs. 8.8(b) and (c) where we show what we call the *Hvorslev – Coulomb* surface in $(\sigma', w, \tau)$ space. This surface applies to a limited range of states *of failure* in the near vicinity (and rather to the dry side) of the critical states.

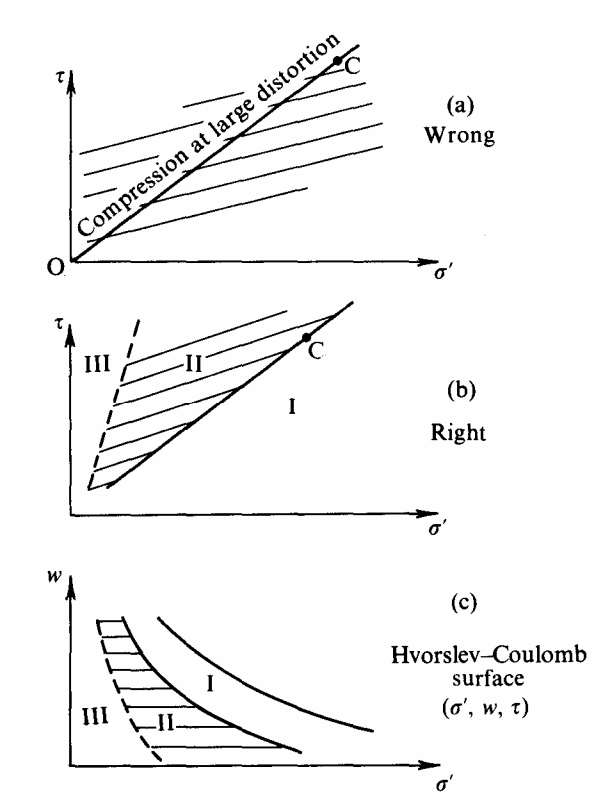


Fig. 8.8 Hvorslev – Coulomb Surface

Hvorslev himself went on from shear box tests to apply his criterion to analysis of some unconfined compression tests. He used $q$ for the axial-deviator stress, and we have adhered to this usage. He suggested that Mises' function $F$ of eq. (2.12) could be employed for soils. We can introduce a generalization of our parameters,

$$(\sigma'_2-\sigma'_3)^2+(\sigma'_3-\sigma'_1)^2+(\sigma'_1-\sigma'_2)^2=2q^{*2}$$

and

$$(\sigma'_1+\sigma'_2+\sigma'_3)=3p^*$$

and appendix C generalizes the Granta-gravel yield function in a form $F(p^*, v, q^*)=0$ that fulfils Hvorslev's suggestion. However, we also see that such yielding occurs in region I of Fig. 8.8 whereas we associate Coulomb's rupture with region II.

## 8.3 Principal Stress Ratio in Soil about to Fail

The Hvorslev – Coulomb surface specifies stress components only on the failure plane. From chapter 2 and appendix A we readily appreciate that this does not fully specify all the principal effective stress components in the soil continuum when it is yielding and about to fail. Let us assume that the rupture surface will be acted on by the maximum and minimum principal effective stresses $\sigma'_{max}$ and $\sigma'_{min}$, so that the intermediate principal effective stress can have any magnitude in the range $\sigma'_{max} \rightarrow \sigma'_{min}$ without affecting the equilibrium or the inclination of the failure surface. We still need some additional assumption if we are to calculate the ratio of principal stresses $\sigma'_{max}/\sigma'_{min}$ in soil about to fail.

The first assumption to be considered is that of Rankine, who studied soil without cohesion ($k = 0$) or pore-pressure ($u_w = 0$). He asserted that in a continuous body of soil when the ratio of principal stresses reached its peak the obliquity of the stress vector on any plane could not exceed the angle of friction $\rho$. It followed, as we will see below, that Rankine could write

$$\frac{\sigma'_{\max}}{\sigma'_{\min}} \le \frac{1+\sin\rho}{1-\sin\rho} \tag{8.5}$$

A generalization became possible following the introduction of Mohr's circle of effective stress, see appendix A. For soil with cohesion $k$ and friction $\rho$, introducing the notation

$$H = k\cot\rho \tag{8.6}$$

in Fig. 8.9, we see from the geometry of the figure that

$$\frac{\sigma'_{\max}+H}{\sigma'_{\min}+H} = \frac{\mathrm{JR}}{\mathrm{JP}} = \frac{\mathrm{RN}}{\mathrm{PL}} \quad (\Delta JPL \text{ similar to } \Delta JRN)$$

$$= \frac{\mathrm{RN}}{\mathrm{PL}} \quad (\text{tangents to circle from N and L})$$

$$= \frac{\mathrm{QM}\tan \mathrm{M\hat{Q}N}}{\mathrm{QM}\cot \mathrm{M\hat{L}Q}} \qquad (\text{tangents to circle from N and L})$$

but $\mathrm{M\hat{Q}N} = (\pi/4 + \rho/2) = \mathrm{M\hat{L}Q}$, so

$$\frac{\sigma'_{\max}+H}{\sigma'_{\min}+H} = \tan^2\left(\frac{\pi}{4}+\frac{\rho}{2}\right) = \left(\frac{1+\sin\rho}{1-\sin\rho}\right). \tag{8.7}$$

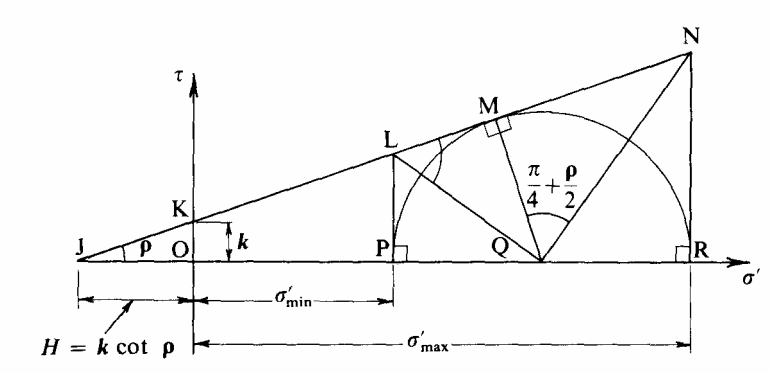


Fig. 8.9 Mohr–Rankine Criterion

Introducing $k = 0 = H$ we find Rankine's earlier expression to be included in eq. (8.7), which we now will call the *Mohr–Rankine* criterion for peak effective stress ratios in soil about to fail.

A distinction has now been made between the peak stress criterion in which the soil body is still considered to be a homogeneous continuum, and the Hvorslev–Coulomb equation for limiting equilibrium between two separate parts of an only just ruptured body. Further, we note that, at the Mohr–Rankine peak stress ratio, there are *two* directions through a soil body of planes on which the obliquities of stress vector are identical. The Mohr–Rankine criterion does not indicate in which of the two directions the Coulomb rupture is expected to be propagated.

A further uncertainty becomes apparent when we try to represent the Mohr–Rankine criterion in the $(q, p)$ plane. At one extreme we have the extension test with the intermediate stress equal to the *major* principal stress, and at the other extreme the compression test where it is equal to the *minor* principal stress. Let us consider the simple case without cohesion, $k = 0$. The first possibility involves failure in extension with $\sigma'_r = \sigma'_{\max}, \sigma'_l = \sigma'_{\min}$, and

$$\sigma'_r = \left(\frac{1+\sin\rho}{1-\sin\rho}\right)\sigma'_l,$$

in which case

$$p = \frac{\sigma'_l + 2\sigma'_r}{3} = \left(\frac{3+\sin\rho}{3-3\sin\rho}\right)\sigma'_l$$

$$-q = (\sigma'_r - \sigma'_l) = \left(\frac{2\sin\rho}{1-\sin\rho}\right)\sigma'_l$$

so that $$\left(\frac{-q}{p}\right)_{\text{peak}} = \frac{6\sin\rho}{3+\sin\rho} \quad (\sigma'_r > \sigma'_l). \tag{8.8}$$

The second possibility involves failure in compression with $\sigma'_l = \sigma'_{\max}$, $\sigma'_r = \sigma'_{\min}$, and

$$\sigma'_l = \left(\frac{1+\sin\rho}{1-\sin\rho}\right)\sigma'_r$$

which gives

$$\left(\frac{+q}{p}\right)_{peak} = \frac{6\sin\rho}{3-\sin\rho} \quad (\sigma'_l > \sigma'_r). \tag{8.9}$$

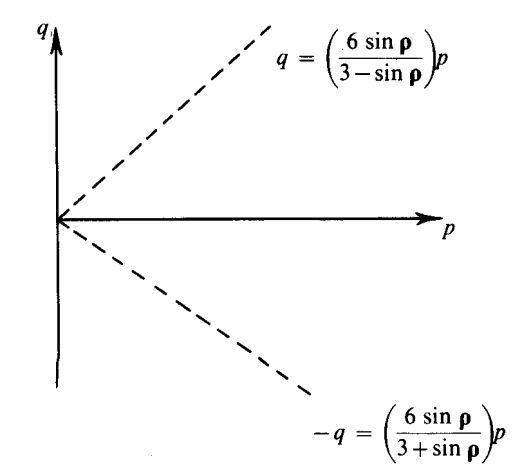


Fig. 8.10 Mohr–Rankine Limiting-stress Ratios

Thus there are two lines which are drawn dotted on the ($q$, $p$) plane, Fig. 8.10, and which indicate states when compression and extension tests respectively reach their peak Mohr–Rankine stress ratio.

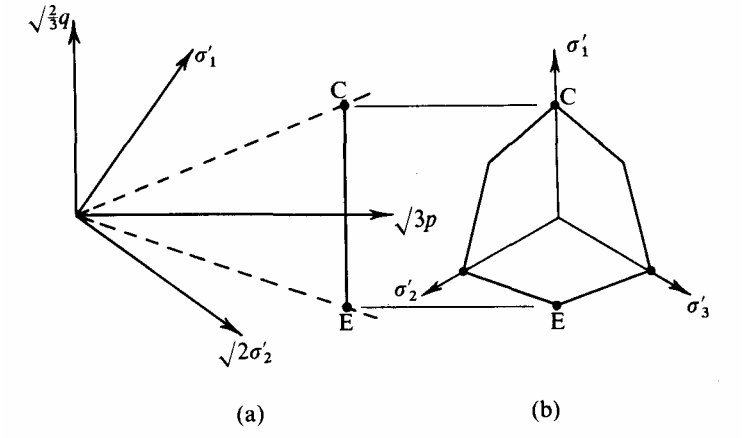


Fig. 8.11 Mohr–Rankine Criterion in Principal Stress Space

If we also want the principal stress space representation we simply convert scales by factors of $\sqrt{\frac{2}{3}}$ and $\sqrt{3}$ , and obtain the dotted lines in Fig. 8.11(a). A section of principal stress space on the plane CE normal to the space diagonal is shown in Figs. 8.11(b) and 8.12. The peak stresses in Fig. 8.12 now lie on an irregular hexagonal cone of an almost triangular section in the plane perpendicular to the space diagonal. Principal points on the Mohr–Rankine peak stress locus are C and E, which refer to peak stress ratios in compression and extension.[5]

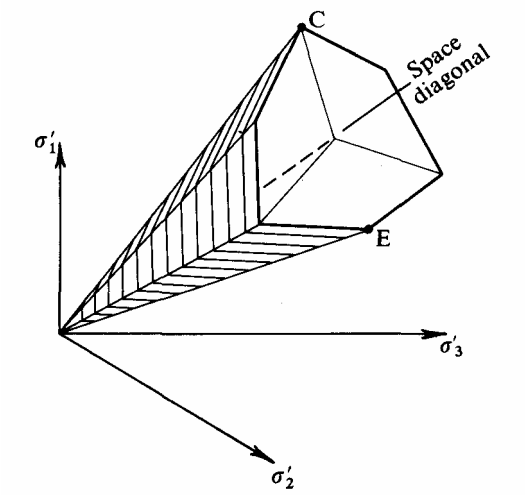


Fig. 8.12 Mohr–Rankine Limiting Surface for **k**=O

The yield surface of Fig. 5.1 is a surface of rotation about the space diagonal which, for states rather drier than critical, lies outside the irregular cone of Fig. 8.12. Thus, the Mohr – Rankine criterion predicts that for these states a limiting stress ratio occurs before the yield surface is reached. We now compare this prediction with some data of states of failure.

## 8.4 Data of States of Failure

We have already discussed the data of experiments which Henkel interpreted to give broad support to Rendulic's generalized effective stress principle. In Figs. 7.22 and 7.23 we see that state paths end with 'failure states' which lie on two lines rather similarly placed in their asymmetry about the space diagonal as the prediction of the Mohr – Rankine criterion. In detail neither a simple critical state curve, nor a simple Mohr – Rankine criterion with constant cohesion, will fit these data of *failure;* it is necessary to have cohesion varying with water content.

In Fig. 8.13 we present data of a comprehensive series of tests on Weald clay reported by Parry.[6] Each point shown is the failure condition (defined by maximum axial-deviator stress $q$) for one separate axial test quoted in Parry's tables. This series includes both compression and extension tests: and in each category three types of drained test ((a) $\sigma'_r$ constant, (b) $\sigma'_l$ constant, (c) $p$ constant), and two types of undrained test ((a) $\sigma_r$ constant (b) $\sigma_l$ constant).

The results have been plotted in the same format as Hvorslev's presentation of Fig. 8.6, except that we have introduced a minor variation in our choice of parameters. Instead of dividing by Hvorslev's equivalent pressure $\sigma'_e$ (or $p_e$) to make the parameters

dimensionless, we have divided by $p_u$ which has exactly the same effect. The effective spherical pressure $p_u$ can be plotted on the critical state line at the particular value of the water content $w_f$ of each separate specimen at failure, whereas a point ($p_e$, $w_f$) could be plotted on the virgin compression line. The actual values adopted for $p_u$ were taken from the similar plot to that of Fig. 7.5 for Weald clay. From chapter 6 we have already established that the ratio $p_e / p_u = \exp \Lambda$ and should be constant for any particular clay.

We see that although these data of failure are from a wide variety of tests (with significantly different stress paths) they are closely represented by a pair of lines of the Mohr – Rankine type of Fig. 8.10,

$$\frac{\sigma'_{\max} + H}{\sigma'_{\min} + H} = \frac{1 + \sin\rho}{1 - \sin\rho} = 1.95$$

where $H = 0.2 p_u = 0.107 p_e$ and $\rho = 18^\circ 47'$.

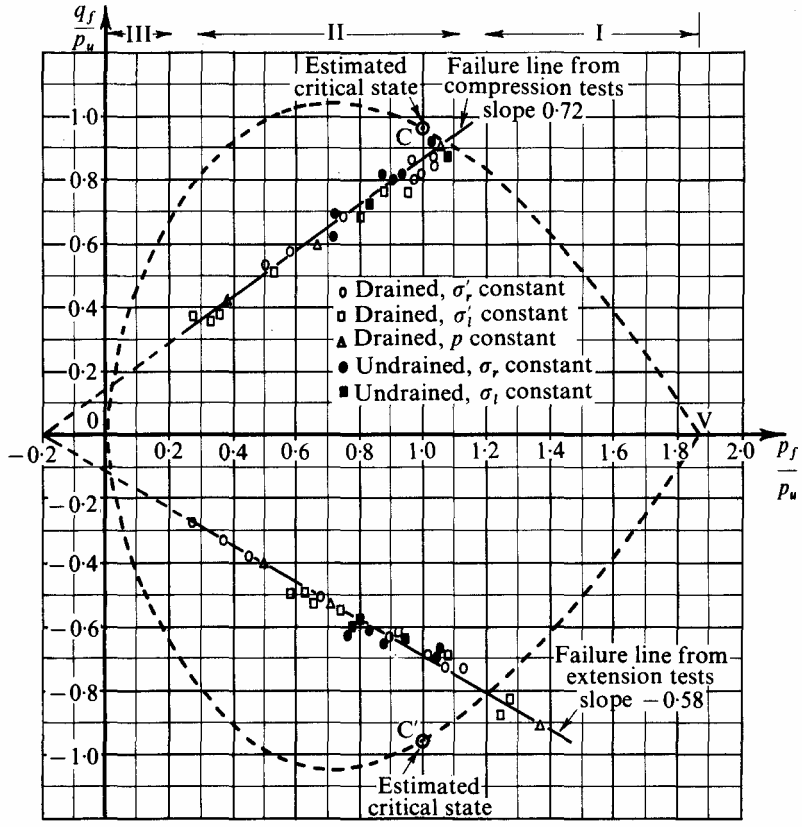


Fig. 8.13 Data of Failure from Tests on Weald Clay (After Parry)

The line for compression is from eq. (8.9)

$$\frac{+q_f}{p_f + 0.2 p_u} = \frac{6 \times 0.322}{3 - 0.322} = 0.72 \tag{8.10}$$

and the line for extension is from eq. (8.8)

$$\frac{-q_f}{p_f + 0.2 p_u} = \frac{6 \times 0.322}{3 + 0.322} = 0.58 \tag{8.11}$$

and the line for extension is from eq. (8.8)

$$\frac{-q_f}{p_f + 0.2 p_u} = \frac{6 \times 0.322}{3 + 0.322} = 0.58 \tag{8.11}$$

The closeness of the fitting suggests that we can extend Hvorslev's concept of cohesion as a function of specific volume (or water content), and introduce this concept also in the Mohr – Rankine peak stress ratio criterion.

As before, there is a range II of $p_f / p_u$ to which the failure criterion is applicable, and to either side there are ranges I and III in which there are no data of *failure:* although the positions of the exact boundaries to range II are open to some doubt.

Also plotted is the section of the boundary surface appropriate to Weald clay which has an average $\kappa = 0.0346, \lambda = 0.093, \text{and } M = 0.95.$ This gives $\Lambda = 0.628$ and $p_e / p_u = \exp \Lambda = 1.875.$ With the exception of three results from extension tests this curve encloses all the data. (Extension tests are more susceptible to experimental error than conventional compression tests, particularly in regard to estimates of water content at failure $w_f$. Any error in $w_f$ leads to a wrong choice of $p_u$ which would move a plotted point directly towards or away from the origin of coordinates O.)

This use of the Coulomb equation to fit data of failure is close in essence to Hvorslev's use of the same equation with cohesion as a function of water content. We will not offer a theoretical explanation for the closeness of this fitting, but it is helpful to compare and contrast Figs. 8.13, 7.12, and 5.18. We began with a theoretical rigid/plastic model for which we predicted rigidity within a certain area of Fig. 5.18: we supposed that in a certain area of that figure stable yielding could progress towards an ultimate critical state. We learn from experiments that stable yielding does occur in the undrained axial test but in Fig. 7.12 we see failure intervene just before the specimen reaches a critical state. Now we find that lines such as those in Fig. 8.13 cut across the area of rigidity in Fig. 5.18, and these lines mark the *peak* stress ratios that can be attained.

Perhaps it is helpful here to draw an analogy with the simple theory of buckling of struts in which experiments on real struts terminate at peak loads less than the limiting loads predicted by simple elastic theory.

## 8.5 A Failure Mechanism and the Residual Strength on Sliding Surfaces

So far we have shown, for intact soil specimens, that the Mohr – Rankine or Hvorslev – Coulomb criteria do describe the limiting condition just before propagation of a failure surface. We now must consider what happens at and after such failure.

Consider in Fig. 8.14 the state path AB which Hvorslev's clay could have followed if it had been homogeneously remoulded at constant $\sigma'$. The portion AB represents deformation of the intact specimen before peak stress. The fact that when Hvorslev sampled water content he did not find all circled points in Fig. 8.4(a) lying close to the critical states, but rather found water contents such as B in Fig. 8.14(b), shows that the specimens stopped behaving uniformly at peak deviator stress. Photographs showed very thin slip zones or rupture surfaces in which most distortion became concentrated after failure. We show, in Fig. 8.15(a), the water content slice and, in Figs. 8.15(b), (c), a much magnified view of the 3 mm thick slice. Figure 8.15(b) shows homogeneous distortion and

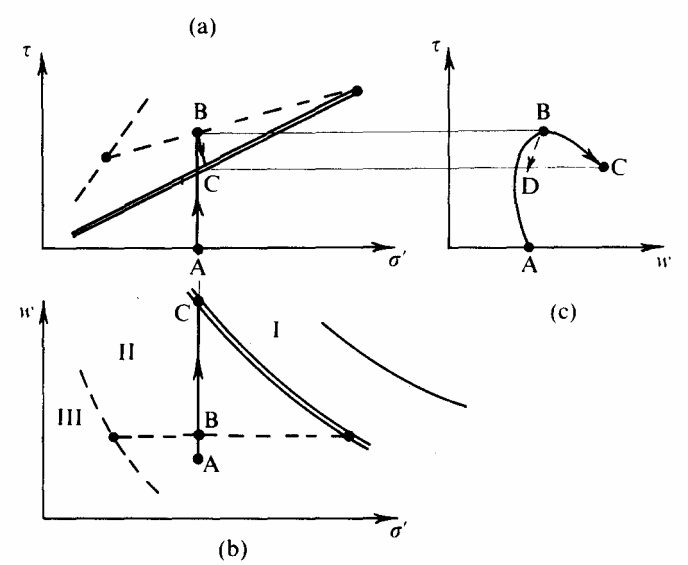


Fig. 8.14 Change in State at Failure in Drained Shear Test

uniform water content just *before* failure. Upon failure, soil in the thin slip zone experiences dilation (increase of water content) and *weakens* (decrease of shear strength $\tau$ ) following path BC in Fig. 8.14(c). The gain in water content of the failure region is *temporarily* at the expense of the blocks to either side of the failure surface, which experience loss of water and increase of *stiffness* as the stress decreased following path BD in Fig. 8.14(c). Consequently, displacements are concentrated in the thin failure zone and Fig. 8.15(c) also shows water content change in the vicinity of the failure. Water is shown

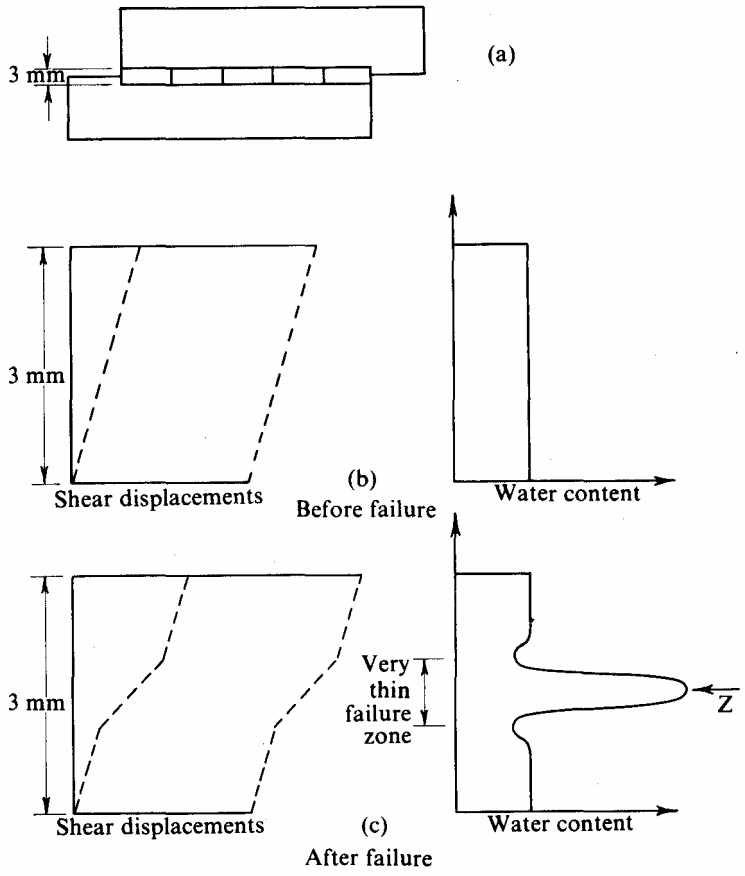


Fig. 8.15 Conditions in a Slip Zone

being sucked, with presumably a small value of pore- pressure, in towards the slip zone Z, but Hvorslev's rapid dismantling process ensured that the average water content that he measured represented the water content just before and at failure. By this interpretation the Hvorslev – Coulomb equation applies to peak stress ratios of an intact soil body.

The sucking in of water towards the thin slip zone, illustrated in Fig. 8.15(c), has been observed in the field. In an investigation of a retaining wall failure (which will be discussed at length in §8.8) Henkel reported the water content variation shown in Fig. 8.16,

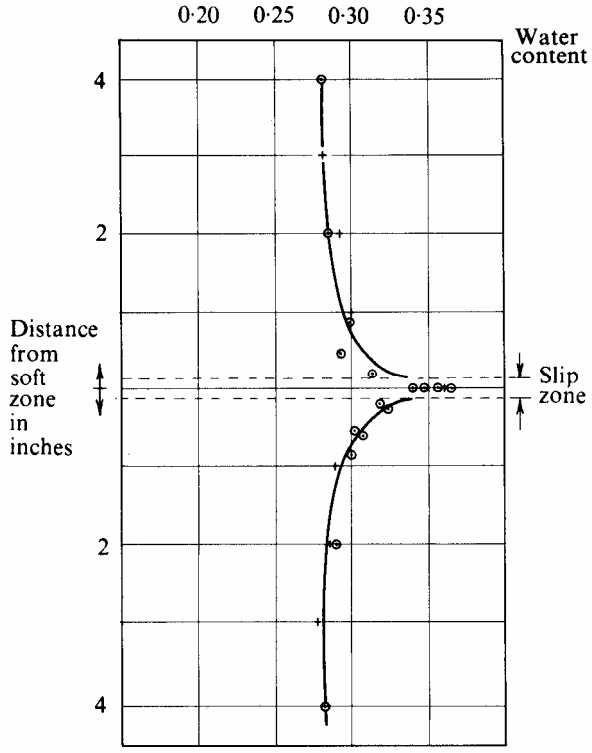


Fig. 8.16 Observations of Water Content of a Slip Zone (After Henkel)

and associated this with local dilation accompanying severe local shear strains. It is consistent with our critical state theories to link the changing water content with fall of stress from peak values (on the dry side) to critical state values.

As displacement on the rupture surface increases there appears to be some development of anisotropy: Hvorslev writes of a significant permanent change of structure in the vicinity of the rupture surface, which permitted one clay sample to be separated into two blocks along the rupture surface which was then seen to possess a dull shine.

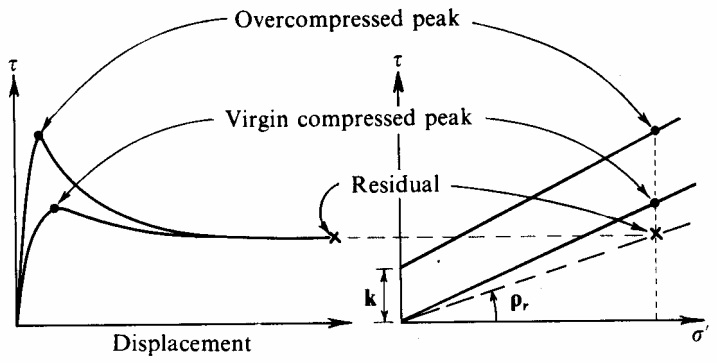


Fig. 8.17 Skempton's Definition of Residual Strength

Gould[7] studied landslides in coastal California and from their evident limiting equilibrium concluded that 'the strength actually mobilized in slides or mass creep is inversely proportional to the amount of displacement which has occurred previously in the shear zone'. He considered that 'the means by which large shear strain eliminates true cohesion is not clear', but writes of a 'pattern of irregular slick surfaces'. Wroth8 studied the strength of randomly packed 1 mm steel balls in simple shear, and found that after very large cumulative shear distortion the ultimate strength fell to two-thirds of the critical state strength, and this deterioration of strength was seen to correspond to a development of regularity of packing in the material. Hence, although it is consistent with our critical state concepts to predict a fall of strength from peak values (on the dry side) to critical state values, it is also clear that large displacements on sliding surfaces have to be associated with a further fall below the critical state values.

Skempton[9] (in the fourth Rankine lecture of the British Geotechnical Society in 1964) discusses the fall of strength, and a figure such as his Fig. 6 (our Fig. 8.17) shows the typical curves relating increasing displacement to fall of strength from peak values to what he identifies as a *residual strength* value. He also correlates fall of strength with passage of time after failure, but it is more consistent with our purely mechanical interpretation of the yielding of soil for us to follow Gould and associate fall of strength only with displacement on the rupture surface. Skempton shows (Fig. 8.17) a line of peak strengths of overcompressed soil which we reproduce in Fig. 8.18(a) as the line ABC, and a line of residual strengths which we reproduce as the line OEF. Between these lines Skempton interposes a line of peak strengths of virgin or lightly overcompressed soil. We see in Fig. 7.12 that the peak strength of axial compression tests of such soil occurs just before the critical state is reached. We wish to introduce in Fig. 8.18(a) a line ODC which corresponds to the critical state strengths.

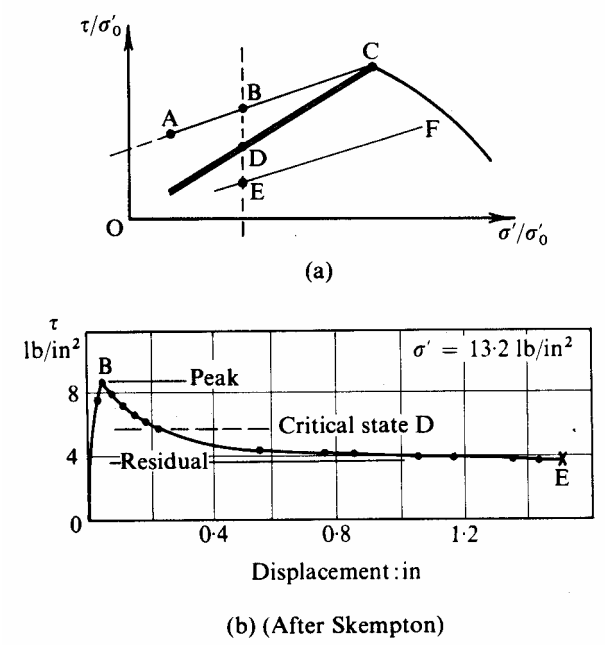


Fig. 8.18 Definition of Critical State Strength

The introduction of line ODC in Fig. 8.18(a) is based simply on our desire to approach this problem from a point of view that is consistent with our critical state theories. As soon as we attempt to define precisely the slope of the line ODC we find a deficiency in the existing development of our theories in that the symbols $\tau$ and $\sigma$' have

not appeared so far. To fit the Mohr-Rankine limiting surface of Fig. 8.12 to conditions in the rupture zone we must take $k = 0$ for soil in the critical state, so that $\tau = \sigma' \tan \rho$. We see that the peak of the undrained axial compression test of Fig. 7.12 occurs when $q/p \cong M$, so to fit $\rho$ to the critical state we must, for example, use

$$\frac{q}{p} = M = 0.88 \qquad \text{for London clay,}$$

together with eq. (8.9)

$$\frac{6 \sin \rho}{3 - \sin \rho} = \left( \frac{q}{p} \right)_{\text{peak}} \cong M = 0.88$$

to give

$$\sin \rho = 0.383, \quad \rho = 22\tfrac{1}{2}^{\circ}, \qquad \text{for London clay}^{10}.$$

This gives $\tan \rho = 0.415$ and in Fig. 8.18(a) the line ODC has been drawn at the slope

$$\frac{\tau}{\sigma'} = 0.415$$

In Fig. 8.18(b) we show Skempton's curve for the fall of strength of weathered London clay at Hendon, with $\sigma' = 13.2\,\text{lb/in}^2$. For this we calculate

$$\tau = 0.415 \qquad \sigma' = 5.5\,\text{lb/in}^2$$

which is plotted in Fig. 8.18(b). It lies about half-way between Skempton's peak value and his residual value. Skempton himself introduces a residual factor $R$ for interpolation between these extremes. It seems that our use of a critical state theory agrees well with the use of a residual factor that Skempton proposes in this case.

As the overcompression ratio increases, the line BDE in Fig. 8.18(a) will move nearer the origin with the consequence that the ratio (BD/BE) will increase. This suggests the use of a residual factor that increases with overcompression ratio $N$.

## 8.6 Design Calculations

In order to help us to stand back from the close detail of interpretation of data, and to take a rather more broad view of the general problems of design, let us review the well-known calculations that occur in structural engineering design. Design of a structure such as a welded steel portal frame, Fig. 8.19(a), can involve two stages of calculation. In one stage, Fig. 8.19(b), some simple calculations are made of the collapse of the frame under various extreme loadings, and the design consideration might be that when the expected working loads are increased by a load factor (for example this might be 2) the structure should not quite collapse. In another stage, Fig. 8.19(c), other calculations are made of the performance of the frame under various working conditions, and the design consideration might be that the deflections or perhaps the natural period of vibration of the structure should be within certain limits. At one stage of the design the steel is represented by a rigid/plastic model with a characteristic yield strength (fully plastic moment $M_p$ in Fig. 8.19(e)). At another stage of the design the steel is represented by an elastic model with a characteristic elastic stiffness ($EI$ in Fig. 8.19(f)). Experimental moment-curvature data for the steel, Fig. 8.19(d), are such that one model applies in one range of the data and another model applies in another range. Each design calculation illuminates one aspect of performance of the structure, and both are of importance to the designer.

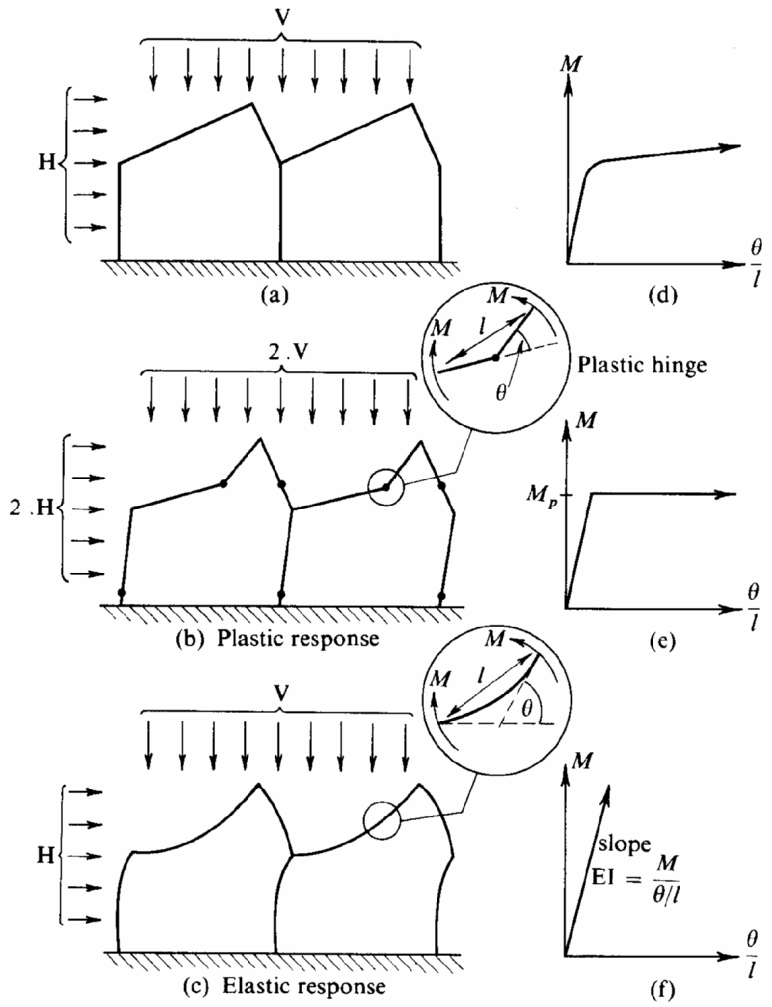


Fig. 8.19 Design of Steel Portal Frame

In soil mechanics we also have a variety of calculations that are appropriate to various aspects of design. Each calculation involves a well defined model such as those discussed in chapters 3 and 4, and the engineer must choose values for parameters such as permeability or compressibility that are appropriate to each specific soil. There is a well known and extensive set of classical calculations of limiting equilibrium based on Coulomb's equation, and Bishop and Bjerrum2 have discussed in a joint paper two different types of problem concerning the performance of loaded bodies of soil for which these classical calculations are appropriate, provided that the strength parameters (***k***, ρ) are chosen in a rational manner. It is usual to introduce a *factor of safety* to cover inadequacies in the design calculations. In a passage of his 1776 paper Coulomb expressed a wish that his retaining wall design should offer a resistance 'd'un quart en sus de celle qui seroit nécessaire pour l'équilibre' (a quarter above what is needed for equilibrium). Thus Coulomb used a load factor of 125, and today, in slope stability calculations, engineers adopt a similar value for a factor of safety applied to the chosen strength parameters. This is a low value which is clearly not appropriate to a peak strength such as is shown in Fig. 8.18, but which does appear to be appropriate to critical state strengths.

The two types of problem are:

I. The *immediate* problem of the equilibrium of soft 'wet' soil under rapidly applied loading. The whole soil mass yields as a perfectly plastic body with positive pore-pressure being generated throughout the interior (the significant lengths $H$ of drainage path are of the same order as the overall dimensions of the body and the half- settlement times are long in comparison with typical loading times). Bishop and Bjerrum quote many cases for which the classical calculations with values (which are in effect critical state strengths)

$$k = c_u \quad \text{and} \quad \tan\rho = 0 \tag{8.12}$$

are clearly appropriate.

II. The *long-term* problem of the equilibrium of firm 'dry' soil. Under an increase of deviatoric stress without increase of effective spherical pressure, the whole soil body may rupture into a rubble of lubricated blocks (the significant lengths $H$ of drainage paths are of the same order as the thickness of a slip zone). In typical cases the loading is sustained for a sufficient time for the conditions of the problem to become effectively 'drained' in the sense suggested in §4.6. Bishop and Bjerrum quote cases of long-term failure for which classical calculations *either* with values

$$k = 0 \quad \textit{and} \quad \frac{6\sin\rho}{3 - \sin\rho} = M \tag{8.13}$$

*or* with $k = 0$ and $\rho$ at some suitable *residual* value would have been appropriate in design.

In identifying these two groups of problems, Bishop and Bjerrum drew on a wide experience of many case histories. We will not repeat their list of cases but will concentrate on two examples of failures which are well documented in the literature of the subject.

## 8.7 An Example of an Immediate Problem of Limiting Equilibrium

At a building site between Stirling and Glasgow in Scotland, during the construction of the roof of a single-storey building, the most heavily loaded footing failed and caused structural damage. Calculations subsequently showed[11] that this footing, at a depth of about 5 ft 6 in below ground level, had applied a net increase of pressure of about 2500 lb/ft$^2$ on an underlying layer of about 14 ft of soft clay. In the site investigation Skempton took small undisturbed cylindrical samples of the soft clay and tested them in rapid unconfined compression; the results, shown in Fig; 8.20, indicate that the soft clay had strength $c_u$ of about 350 lb/ft$^2$. Skempton used alternative methods of calculation including

(a) limiting equilibrium with cohesion $k$ alone on a slip circle (this type of calculation will be discussed in §9.4), and
(b) limiting equilibrium of a two-dimensional stress distribution in a purely cohesive soil (this type of calculation will be discussed in §9.6.1).

By these methods he estimated the bearing capacity of the clay layer to be about 2300 lb/ft$^2$. With various arguments which it is inappropriate to discuss in detail here, he demonstrated that this estimated bearing capacity correlated well with the increase of pressure that actually caused failure.

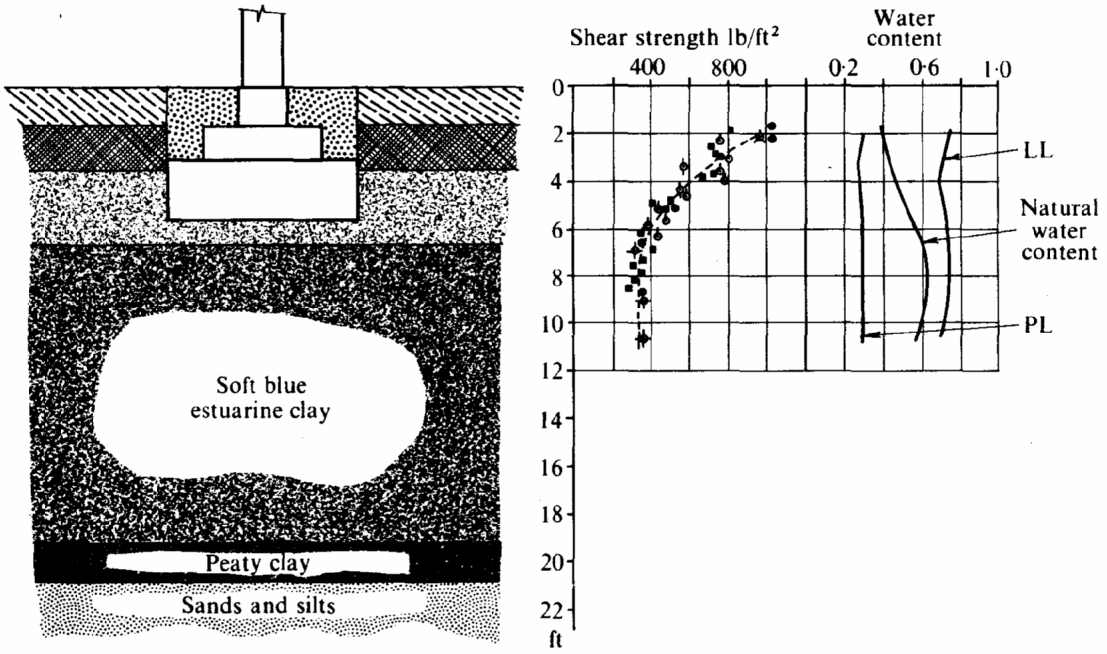


Fig. 8.20 An Example of an Immediate Failure of Bearing Capacity (After Skempton)

We need to review the reasons why, in this case, the immediate limiting equilibrium calculation using $k=c_u$, $\rho = 0$, was appropriate. In the first place the calculated amount of consolidation which took place in the few months of construction was negligible. The clay was compelled to deform at the same constant specific volume as it had initially, and whatever pore-pressures were generated would have had no time to dissipate. Second, although the clay might have been slightly overcompressed, the possible undrained test paths as shown in Fig. 7.28(a) all come to an end near the ultimate critical state point C. In the fully deformed state any history of overcompression would have been eradicated and the *effective* spherical pressure would have come close to the critical state value in Fig. 7.28(a). The *total* pressures could then be whatever values were applied, since any change in total pressure would simply cause variation of pore-pressure. (We know that *total* pressure cannot generate friction in an analogous situation when we accidentally tread on a bladder full of water, such as a rubber hot-water bottle. The weight on the foot generates water pressure but there is little pressure generated between the internal faces of the bladder so that there is little friction.) In Fig. 7.26 we see that $q_u = Mp_u$; the strength has a frictional character but it depends on the mean effective spherical pressure $p_u$ in the deforming clay. The total pressure cannot alter the mean effective pressure unless there is some change in the specific volume, $v_0$ in Fig. 7.25. So the limiting equilibrium calculation proceeds on the basis of a constant (low) value of shear strength $k = c_u$, and no friction.

## 8.8 An Example of the Long-term Problem of Limiting Equilibrium

It is less easy to find good text-book examples of the drained than the undrained limiting equilibrium problem. Our choice of a retaining wall failure is dictated by the ease with which the original paper[12] can be found and the clarity with which the description and discussion[13] is developed.

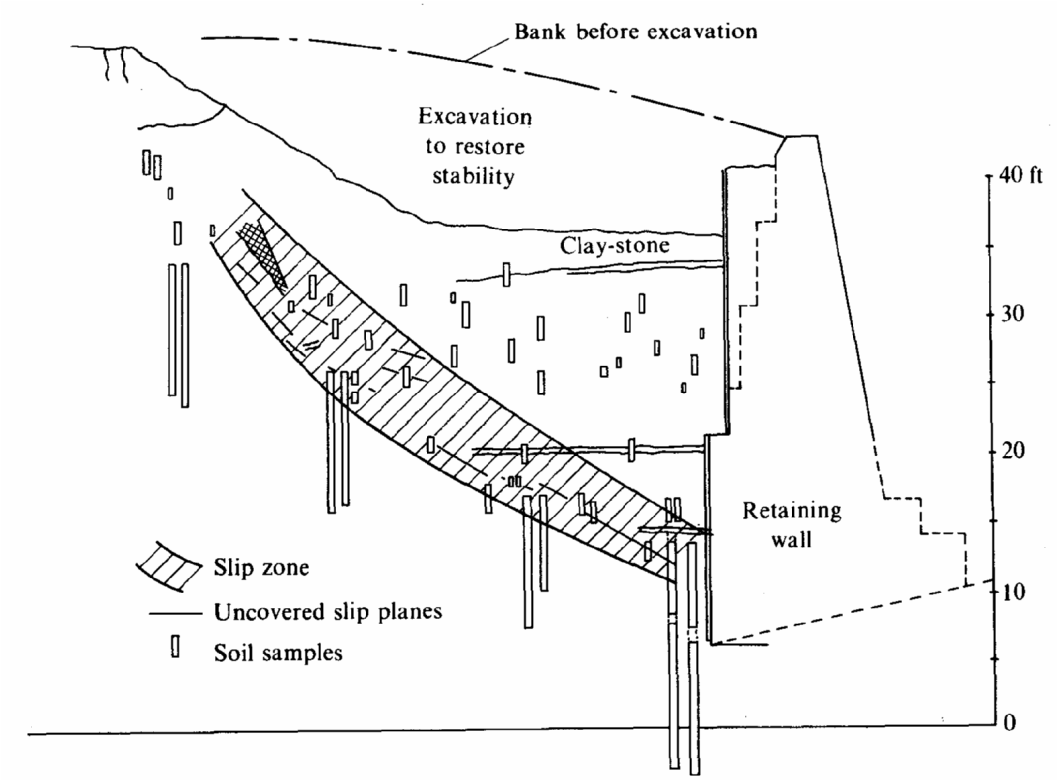


8.21 An Example of Long-term Failure of Retaining Wall (After Watson)

A railway cutting was made in 1912 through a gently sloping clay hill near Uxbridge, which is a suburb of London. Since then there has been a history of intermittent slips; and in 1937 when the railway was widened and a new retaining wall built, a serious slip occurred during its construction. The slope behind the wall cracked and was made good with hard-core rubble to support some houses at the top of the slope. In 1954 another serious slip broke the wall, and renewed cracks at the head of the slope made it necessary to demolish the houses. Forward movement of the toe of the wall menaced the railway tracks but promptly executed remedial works arrested movement and restored stability. The paper shows, Fig. 8.21, the findings of a site investigation by means of a trench cut into the slope. The stiff fissured London clay contained an inclined layer within which there were many thin slip zones which are seen to be *not* continuous. These thin slip zones were 'clearly exposed since large chunks of clay slipped away when digging near the surfaces, which appeared to consist of very thin moist slide-surfaces with marks of relative movement rather than softened zones'. Borings were put down in an endeavour to find these 'moist slide-surfaces', but examination of several samples known to be driven across slide-surfaces uncovered in the trench failed to locate the surfaces in the laboratory. Only in one sample did the moist zone attain sufficient thickness (about 50 mm) for increase of water content to show the results already indicated in Fig. 8.16. (Even at that thickness the remoulded softened clay paste in the slip zone remains 'drained' rather than 'undrained' in relation to the time of construction and loading.)

Henkel reported in the discussion the results of limiting equilibrium calculations which used straight slip surfaces in a manner outlined in the examples of §9.1 and §9.2. Henkel's choice of parameters was the value of $\rho = 20°$ that he found from an interpretation of data of peak-strengths of London clay specimens in the manner of §8.4, but he then found that the value of $\boldsymbol{k}$, which could have been contributing to stability of the ground which actually failed, was less than the peak value. In §8.6 from eq. (8.13) we suggest the comparable critical state parameters $\boldsymbol{k} = 0$ and $\rho = 22½°$ for London clay.

When such failure first takes place the body of clay disintegrates into a rubble of lubricated blocks, sliding on each other on very thin moist zones of soft, lubricating clay paste. Critical state theory explains the failure mechanism, and also gives us the key to the behaviour of this lubricating clay paste. The soft clay is being severely remoulded but it can only soften to the critical state that corresponds with its effective spherical pressure. This pressure, and the corresponding critical state strength, increase with depth in the rubble. The 'friction' concept involves a resistance to relative motion that depends on the effective stress between blocks. We can apply the well established friction calculations to the limiting equilibrium of a slipping rubble of clay blocks only because the strength with which the blocks adhere to each other is proportional to the pressure that has long been effective between them.

## 8.9 Summary

In chapter *5* we began asking what state of effective stress could be sustained in stable equilibrium by a block of our first model soil. We then developed a new group of critical state theories of yielding of soil but found that as yielding progressed there came a stage at which soil specimens in actual test systems 'failed' before they could be brought into a critical state. The data of peak strengths proved to be capable of very close description by the Coulomb equation, when properly modified to account for the effect of water content changes on cohesion. However, in classical calculations of limiting equilibrium for design purposes, it proves rational in general to use strength parameters ***(k,*** ρ) that are based on the critical state model rather than on the peak strengths. In chapter 9, the actual classical calculations of limiting equilibrium are given attention.

*References to Chapter 8*


1. Coulomb, C. A. Essai sur une application des règles de maximis et minimis a quelques problèmes de statique, relatifs a l'architecture, *Mémoires de Marhématique de l'Académie Royale des Sciences,* Paris, 7, 343 – 82, 1776.
2. Bishop, A. W. and Bjerrum, L. The Relevance of the Triaxial Test to the Solution of Stability Problems, *Res. Conf. on Shear Strength of Cohesive Soils, A.S.C.E.,* Boulder, pp. 437 – 501, 1960.
3. Hvorslev, M. J. *(Iber die Festigkeitseigenschaften Gestörter Bindiger Böden,* Køpenhavn, 1937.
4. Schofield, A. N. and Togrol, E. Critical States of Soil, *Bulletin of the Technical University of Istanbul,* 19, *39 – 56,* 1966.
5. Kirkpatrick, W. M. *The Behaviour of Sands under Three-dimensional Stress Systems,* Ph.D. Thesis, Glasgow University, 1954.
6. Parry, R. H. 0. Triaxial Compression and Extension Tests on Remoulded Saturated Clay, *Géotechnique,* 10, 166 – 80, 1960.
7. Gould, J. P. A Study of Shear Failure in Certain Tertiary Marine Sediments, *Res. Conf on Shear Strength of Cohesive Soils, A.S.C.E.,* Boulder, pp. 615 – 41, 1960.
8. Wroth, C. P. *Shear Behaviour of Soils,* Ph.D. Thesis, Cambridge University, 1958.
9. Skempton, A. W. Long-term Stability of Clay Slopes, *Géotechnique,* **14,** 77 – 101, 1964.
10. Burland, J. B. Reply to discussion in *Large Bored Piles,* Inst. Civ. Eng., London, p. 102, 1966.
11. Skempton, A. W. An Investigation of the Bearing Capacity of a soft Clay Soil, *J.I.C.E.,* 18, 307 – 21, 1942.

[12] Watson, J. D. Earth Movement affecting L.T.E. Railway in Deep Cutting East of Uxbridge, *Proc. Inst. Civ. Eng.,* Pt II, 5, 302 – 31, 1956.

[13] Henkel, D. J. Discussion on 'Earth Movement affecting L.T.E. Railway in Deep Cutting East of Uxbridge', *Proc. Inst. Civ. Eng.,* Pt II, *5,* 320 – 3, 1956.